Vertical Electrical Conductivity of ZnO/GaN Multilayers for Application in Distributed Bragg Reflectors

Filip Hjort , Ehsan Hashemi, David Adolph, Tommy Ive, Olof Bäcke, Mats Halvarsson, and Åsa Haglund

Abstract—We have demonstrated an electrically conductive ZnO/GaN multilayer structure using hybrid plasma-assisted molecular beam epitaxy. Electrical *I-V* characteristics were measured through the top three pairs of a six pair ZnO/GaN sample. The total measured resistance was dominated by lateral and contact resistances, setting an upper limit of $\sim 10^{-4}\,\Omega\cdot cm^2$ for the vertical specific series resistance of the stack. A strong contribution to the low resistance is the cancellation of spontaneous and piezoelectric polarization that occurs in the in-plane strained ZnO/GaN sample, as shown by electrical simulations. In addition, the simulations show that the actual vertical resistance of the sample could in fact be three orders of magnitude lower and that ZnO/GaN structures with thicknesses fulfilling the Bragg condition should have similar resistance. Our results suggest that ZnO/GaN distributed Bragg reflectors (DBRs) are a promising alternative to pure III-nitride DBRs in GaN-based vertical-cavity surface-emitting lasers.

Index Terms—ZnO, GaN, distributed Bragg reflector, electrical conductivity, vertical-cavity surface-emitting laser.

I. INTRODUCTION

VERTICAL-CAVITY surface-emitting lasers (VCSELs) have small-divergence and circular-symmetric output beams, low lasing threshold currents, good 2D-array manufacturing compatibility, and low manufacturing cost due to on-wafer testing. Therefore, infrared-emitting VCSELs are used extensively in e.g. sensing and optical communication. However, III-nitride based VCSELs with emission wavelengths in the UV and visible, which could find applications in pico projectors, head-up and near-eye displays, biomedicine, and visible-light communication [1], [2], are still not commercially available. Several research groups have reported lasing of electrically injected III-nitride VCSELs [3]–[12] but there is still a need to reach higher output powers, lower threshold currents and improved thermal stability.

F. Hjort, E. Hashemi, D. Adolph, T. Ive, and Å. Haglund are with the Department of Microtechnology and Nanoscience, Chalmers University of Technology, 412 96 Gothenburg, Sweden (e-mail: filip.hjort@chalmers.se).

O. Bäcke and M. Halvarsson are with the Department of Physics, Chalmers University of Technology, 412 96 Gothenburg, Sweden.

Until recently [11], all III-nitride based VCSELs had employed electrically insulating distributed Bragg reflectors (DBRs), demanding intracavity contacts. To reduce the lateral resistance, intracavity contacts must be combined with long cavities, resulting in a low longitudinal optical confinement factor and a high optical loss. A conductive n-type DBR would make it possible to place the n-side metal contact outside the cavity and thereby allow for a shorter cavity length. The progress in realizing electrically conductive n-type III-nitride DBRs has been hampered by the large conduction band offsets, the large polarization charges at the interfaces, and the low Al(Ga)N electrical conductivity.

The lowest specific series resistances reported for III-nitride DBRs are $2 \times 10^{-4}\,\Omega\cdot cm^2$ for a 40 pair $Al_{0.12}Ga_{0.88}N$/GaN DBR having a 92 % peak reflectivity and 11 nm stopband width [13], and $7.8 \times 10^{-4}\,\Omega\cdot cm^2$ for a 40 pair DBR using lattice-matched $Al_{0.82}In_{0.18}N$/GaN and having a peak reflectivity of 99.9 % and a 22 nm stopband width [11], [14]. The narrow stopband widths are a result of the large number of pairs needed to achieve high reflectivity, due to the relatively small refractive index contrasts for the AlInN/GaN and the low Al-composition AlGaN/GaN material pairs. Electrically conductive high Al-composition Al(Ga)N/GaN DBRs have also been demonstrated [15]–[18], but the specific series resistances, which were in the order of $0.1\,\Omega\cdot cm^2$ or above, are still too high for VCSEL applications, which demand a DBR resistance below roughly $10^{-3}\,\Omega\cdot cm^2$. The only electrically conductive mirror incorporated into a working electrically injected III-nitride VCSEL is the AlInN/GaN DBR developed at Meijo University [11], [14]. Efforts have also been made to make vertically conductive DBRs using n-GaN/GaN where the highly doped n-GaN layers are selectively porosified [19]–[21]. Peak reflectivities of up to $\sim$99.5 % have been achieved for these nanoporous DBRs. The vertical specific series resistance has either been in the order of $1\,\Omega\cdot cm^2$ [21], or no vertical *I-V* characteristics have been presented which makes it difficult to make a fair comparison with other conductive DBRs [19], [20].

A promising alternative to pure III-nitride DBRs is the ZnO/GaN material pair, which has a similar refractive index contrast [22], [23] and a smaller lattice mismatch (1.9 %) [24], [25] compared to AlN/GaN. Due to the large refractive index contrast, only approximately 20 DBRs pairs are needed to achieve above 99% reflectivity which also
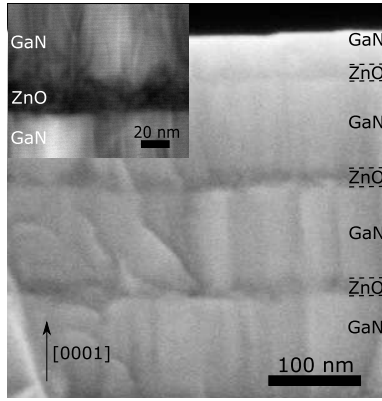
Fig. 1. Scanning electron microscope image showing the top three ZnO/GaN periods. The inset shows a bright field scanning transmission electron microscope image of one ZnO/GaN period.

Fig. 2. Reciprocal space map for the asymmetric $(10\bar{1}5)$ reflection of the six pair ZnO/GaN sample, with the dashed line marking the position of the GaN $(10\bar{1}5)$ reflection.

gives a relatively large stopband width. In addition, ZnO can, as opposed to AlN, easily be doped to high electron concentrations [26] which together with the small conduction band offset of approximately 0.2 eV [27] make ZnO/GaN suitable for vertical electrical injection. As will be shown here, the vertical resistance is further reduced by the cancellation of spontaneous and piezoelectric polarization in in-plane strained DBRs. We recently demonstrated the growth of ZnO/GaN DBRs using hybrid plasma-assisted molecular beam epitaxy (PAMBE) [28]. As a continuation of this work and following preliminary electrical studies [29], we here investigate the vertical electrical conductivity of a six pair ZnO/GaN multilayer structure in detail, both experimentally and through simulations.

II. GROWTH

An n-type and crack-free multilayer sample with six ZnO(0001)/GaN(0001) pairs was grown on a semi-insulating GaN(0001)/Al$_2$O$_3$ substrate by hybrid PAMBE, i.e. both materials were grown in the same chamber. Each layer was grown using a low-temperature followed by a high-temperature growth step, which for ZnO were 300°C and 500°C, and for GaN 500°C and 635°C. For more details on the growth, see [28]. The root-mean-square surface roughness at the top of the 6 pair sample was determined by atomic force microscopy to be 2.1 nm over 2 μm × 2 μm. Hall measurements on samples with only a single layer of either ZnO or GaN showed electron concentrations of 1×10^{19} cm^{-3} for ZnO and 1.8×10^{18} cm^{-3} for GaN. Secondary ion mass spectrometry (SIMS) of ZnO grown on GaN revealed a hydrogen concentration in the order of 10^{20} cm^{-3} and SIMS of GaN grown on ZnO showed oxygen concentrations of $\sim 10^{20}$ cm^{-3}. Concentration of other impurities as Zn and Si in GaN and Ga in ZnO were significantly lower. Hydrogen in ZnO and oxygen in GaN are known to be shallow donors [30], [31] and are likely the main reasons for the unintentional n-doping of the sample.

A scanning electron microscope (SEM) image showing the cross-sectional view of the top three pairs, that were electrically characterized, is presented in Fig. 1. The inset
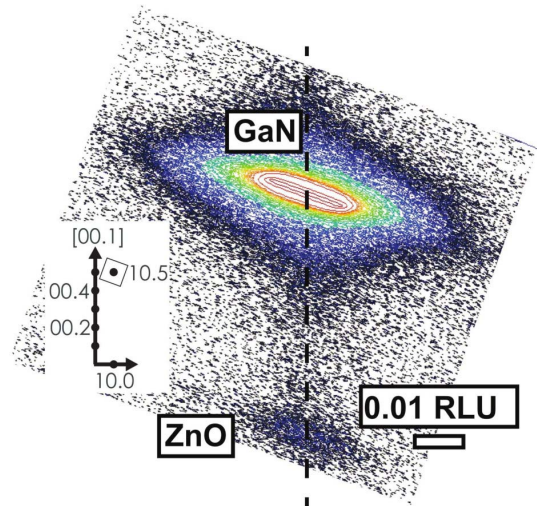
shows a bright field scanning transmission electron microscope (STEM) image of one ZnO/GaN period. The STEM image indicates that the lower GaN/ZnO interface, at the transition from GaN to ZnO in the growth direction, is better defined than the upper ZnO/GaN transition. The target thickness was 56 nm for the ZnO layers and 46 nm for the GaN layers, fulfilling the Bragg condition for a wavelength of 450 nm. Due to an unstable Zn-source, the resulting ZnO layer thicknesses were roughly 20 nm. The GaN layers were between 80 and 110 nm thick as a result of additional GaN growth during temperature ramps. In addition, the topmost GaN layer was only approximately 30 nm thick since substrate heater issues led to an early termination of the growth.

The reciprocal space map for the asymmetric $(10\bar{1}5)$ reflection, measured by x-ray diffraction, is presented in Fig. 2. The ZnO peak is aligned to the GaN peak and the ZnO is thus in-plane strained to the GaN. As we will show later on, this has a large impact on the vertical electrical conductivity of the structure.

III. ELECTRICAL CHARACTERIZATION

In order to measure the vertical resistance, mesa structures with 30, 45, 60, 75 and 100 μm radii were etched and contacted as shown in Fig. 3. Using Cl$_2$/Ar inductively coupled plasma reactive ion etching, three ZnO/GaN pairs high mesa structures were formed. 250 W was used for both the ICP and electrode RF power with 30 sccm Cl$_2$ and 15 sccm Ar flow and 10 mTorr pressure during the 1 minute etch. Inspection of the sample cross-section in the SEM confirmed that the etch had stopped in the GaN layer. Contacts of Al(150 nm)/Pt(50 nm) were deposited by e-beam evaporation at the top and next to the mesas with a lateral distance of 3 μm between the mesa and the top and bottom contact edges, see Fig. 3. Transmission line measurements (TLM) yielded a specific contact resistivity of $\sim 10^{-4}$ $\Omega \cdot$cm^2 and a sheet resistance of the sample of ~ 200 Ω/sq.
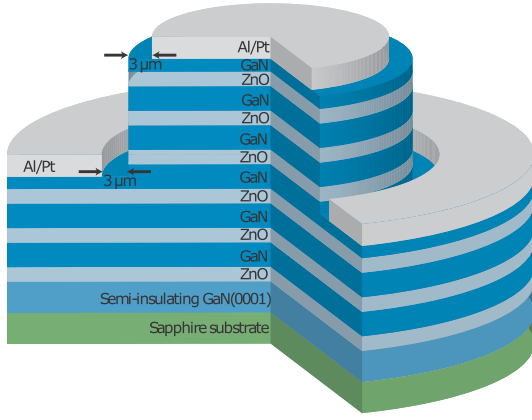
Fig. 3.   Schematic cross-section of the three ZnO/GaN pair high mesas and Al/Pt contacts.
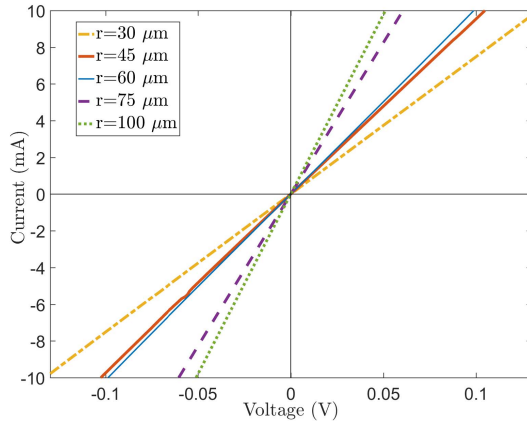

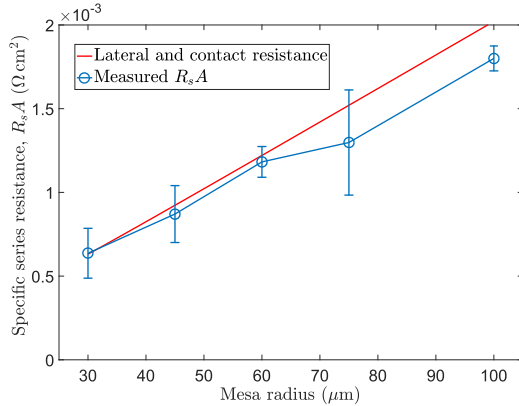Fig. 4.   *I-V* characteristics measured through mesas with three ZnO/GaN pairs of different radii.

Fig. 5.   Mean specific series resistance of three ZnO/GaN pairs with error bars versus mesa radius including an estimation of the contribution from the lateral and contact resistance.

The *I-V* characteristics measured through the top three pairs are linear and shown for different mesa radii in Fig. 4. The specific series resistance, $R_s A$, versus mesa radius is plotted in Fig. 5, where R_s is the series resistance extracted from the *I-V* characteristics and A is the mesa area. By measuring the resistance of mesas with equal radius but at separate locations

on the sample, error bars were calculated. The vertical specific series resistance of the three pairs should not change with mesa radius, assuming the current spreads uniformly over the mesa. In Fig. 5, the specific series resistance is instead increasing approximately linear with mesa radius, corresponding to the case when the contact resistance and the lateral resistance between contact and mesa edge are dominating. The dominance of the lateral and contact resistance was confirmed by estimating their resistance contribution, plotted in Fig. 5, from the TLM measurements. A clear decrease in specific series resistance, when reducing the lateral distance to $3\,\mu$m from $10\,\mu$m used for a previous sample, further confirmed this dominance. Thus, an exact value for the actual vertical resistance cannot be extracted, but the specific series resistance for three pairs, excluding lateral and contact resistance, is at most in the low $10^{-4}\,\Omega\cdot$cm^2 range. The results suggest that a full 20 pair ZnO/GaN DBR should have a specific series resistance comparable to, or lower than, the lowest values reported for III-nitride DBRs.

IV. ELECTRICAL SIMULATIONS

To further investigate the electrical conductivity of ZnO/GaN multilayers, Synopsys' Sentaurus TCAD was used to perform drift-diffusion simulations. It solves the Poisson and carrier continuity equations self-consistently and takes into account tunneling of electrons through the potential barriers. Spontaneous and piezoelectric polarization were included by adding interface sheet charge densities according to [34]

$$\sigma = P_{sp}^{ZnO} - P_{sp}^{GaN} + 2\left(e_{31} - \frac{c_{13}}{c_{33}}e_{33}\right)\frac{a_{GaN} - a_{ZnO}}{a_{ZnO}} + P_{error} \quad (1)$$

where e_{31} and e_{33} are the proper piezoelectric constants for ZnO, c_{13} and c_{33} are elastic constants for ZnO, a_{ZnO} and a_{GaN} are the in-plane lattice constants and P_{sp}^{ZnO} and P_{sp}^{GaN} the spontaneous polarization charge densities for respective material. Recently, Dreyer et al. reported that the common practice to use zincblende as a reference in calculating the spontaneous polarization of wurzite materials and the proper rather than the improper e_{31} piezoelectric constant, gives an error in the calculated total polarization. The term P_{error}, which is especially large for relaxed structures, is added to correct for this [35]. Equation (1) describes the sheet charge density at the passage from fully strained ZnO to relaxed GaN when moving in the growth direction, corresponding to the Zn-face/N-face interfaces. For the O-face/Ga-face interfaces, the sheet charge density has the opposite sign. The material parameter values used in the simulations for ZnO and GaN are listed in Table I together with the material parameter values for AlN.

The band diagram and *I-V* characteristics were simulated for three ZnO/GaN pairs having 80 nm thick GaN and 20 nm thick ZnO layers, and a top 30 nm thick GaN layer, similar to the experimentally characterized top three pairs of the six pair sample. Ideal ohmic contacts at the top and bottom of the stack were used to sweep the voltage bias for current flow simulations. As comparison, simulations for ZnO/GaN and AlN/GaN DBRs with layer thicknesses fulfilling the Bragg condition at a wavelength of 450 nm was also performed.

TABLE I

IN-PLANE LATTICE CONSTANT, a, SPONTANEOUS POLARIZATION CHARGE DENSITY (ZINCBLENDE REFERENCE), P_{sp}, PROPER PIEZOELECTRIC
CONSTANTS, e_{31} AND e_{33}, AND ELASTIC CONSTANTS, c_{13} AND c_{33}, FOR WURTZITE ZnO, GaN, AND AlN [24], [25], [32], [33]

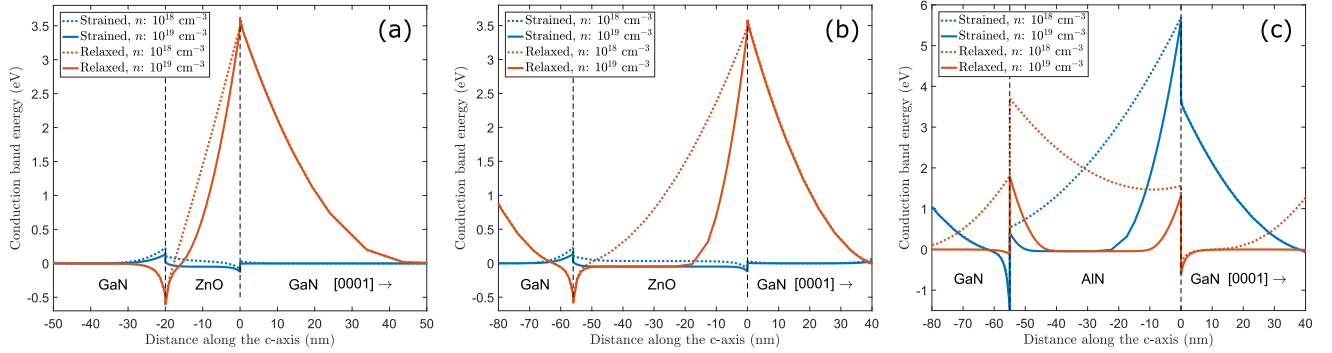| Material	a (Å)	P_{sp} (C/m^2)	e_{31} (C/m^2)	e_{33} (C/m^2)	c_{13} (GPa)	c_{33} (GPa)
ZnO	3.25	-0.057	-0.51	0.89	105	211
GaN	3.19	-0.029	-0.49	0.73	106	398
AlN	3.11	-0.081	-0.60	1.46	108	373

Fig. 6. Simulated conduction band diagram for (a) one ZnO/GaN multilayer period with thicknesses corresponding to the experimentally investigated sample (b) one period of ZnO/GaN with layers thicknesses fulfilling the Bragg condition at 450 nm and (c) an AlN/GaN DBR fulfilling the same Bragg condition. The blue lines are for in-plane strained ZnO and AlN and the red lines for relaxed ZnO and AlN. The dashed lines corresponds to an electron concentration of 10^{18} cm^{-3} in the ZnO and AlN and the solid lines to an electron concentration of 10^{19} cm^{-3}.

Figure 6(a) shows the conduction band diagram for relaxed ZnO and ZnO fully strained to GaN for electron concentrations of 10^{18} cm^{-3} and 10^{19} cm^{-3} in ZnO. An electron concentration of 1.8×10^{18} cm^{-3} is assumed for GaN. Only minor differences are seen when compared with the conduction band diagram for the ZnO/GaN DBR fulfilling the Bragg condition, which is shown in Fig. 6(b). A higher ZnO electron concentration gives a reduction of the potential barrier as the free carriers can screen the polarization sheet charges at the interfaces. The contributions to the sheet charge density from the piezoelectric and the spontaneous polarization almost entirely cancels for the structures with in-plane compressively strained ZnO. As a result, the strained structures have a substantially lower barrier height at the Zn-face/N-face interface compared to the relaxed structures. According to Eq. (1) and Table I, the sheet charge density is 0.0042 C/m^2 when ZnO is strained to GaN and -0.079 C/m^2 for relaxed ZnO, i.e. when there is no piezoelectric polarization. Also for the case of ZnO and GaN both being in-plane strained to an intermediate lattice constant, the two components of the polarizations would cancel. This is in contrast to the case of AlN/GaN for which the conduction band diagram is plotted in Fig. 6(c). With in-plane tensile strained AlN, the strong piezoelectric polarization will give rise to a large total polarization sheet charge density of -0.10 C/m^2 in AlN/GaN DBRs. Together with the larger conduction band offset this results in a significantly higher potential barrier.

Figure 7 shows the vertical specific series resistance, extracted from simulated I-V characteristics, of the ZnO/GaN structure with thicknesses of the experimentally investigated sample. As indicated by the calculated conduction band diagrams, the resistance is strongly dependent upon both electron
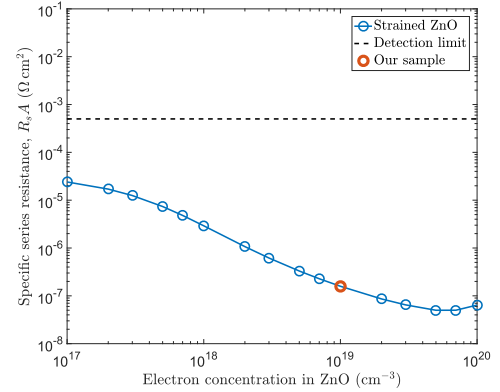

Fig. 7. Specific series resistance simulated for three ZnO/GaN pairs with strained ZnO and different ZnO electron concentrations. The horizontal dashed line indicates the detection limit set by the lateral and contact resistance on our sample and the red circle the electron concentration and simulated specific series resistance of our sample.

concentration and strain. An increased electron concentration in the GaN layers instead of the ZnO layers leads to a similar reduction in resistance, but is not shown in the figure. As expected from the similarity of Fig. 6(a) and Fig. 6(b), only a relatively small difference in resistance was seen compared to the target thicknesses DBR structure. This indicates that samples with target thicknesses should have similar resistance to the sample experimentally investigated here. The red circle illustrates the electron concentration in the experimentally investigated samples as well as the simulated specific series resistance of such a sample. The simulated resistance of $\sim 10^{-7}$ $\Omega \cdot$ cm^2 is more than three orders of magnitude lower than the detection limit set by the lateral and contact

resistance contributions. Thus, the actual vertical resistance of a full 20 pair ZnO/GaN DBR could be as low as $\sim 10^{-6}\,\Omega\cdot\text{cm}^2$, significantly lower than the best reported results for III-nitride based DBRs.

V. Conclusions

We have demonstrated an electrically conductive ZnO/GaN multilayer structure, grown by hybrid PAMBE. We measured an upper limit of the specific series resistance, $R_s A$, for three ZnO/GaN pairs in the low $10^{-4}\,\Omega\cdot\text{cm}^2$ range, comparable to the lowest values reported for III-nitride DBRs. Lateral and contact resistances dominated the total resistance and simulations indicate that the actual vertical specific series resistance of the ZnO/GaN sample could be orders of magnitudes lower. In addition, both GaN and ZnO [26] can easily be doped to high electron concentrations, suggesting that the resistance could be further reduced compared to the unintentionally doped structure investigated here. Although further optimization of the growth is needed to improve especially the optical performance, our results show that ZnO/GaN DBRs are a promising alternative to pure III-nitride n-type DBRs in GaN-based VCSELs. The benefits with this material combination are the large refractive index contrast, small conduction band offset, ease of n-type doping, comparably small lattice mismatch, and, as has been shown here, the cancellation of interface charges induced by piezoelectric and spontaneous polarization.

Acknowledgment

References

[1] D. F. Feezell, "Status and future of GaN-based vertical-cavity surface-emitting lasers," *Proc. SPIE*, vol. 9363, p. 93631G, Mar. 2015.
[2] Å. Haglund *et al.*, "Progress and challenges in electrically pumped GaN-based VCSELs," *Proc. SPIE*, vol. 9892, p. 98920Y, Apr. 2016.
[3] T.-C. Lu, C.-C. Kao, H.-C. Kuo, G.-S. Huang, and S.-C. Wang, "CW lasing of current injection blue GaN-based vertical cavity surface emitting laser," *Appl. Phys. Lett.*, vol. 92, no. 14, p. 141102, Apr. 2008.
[4] Y. Higuchi, K. Omae, H. Matsumura, and T. Mukai, "Room-temperature CW lasing of a GaN-based vertical-cavity surface-emitting laser by current injection," *Appl. Phys. Express*, vol. 1, no. 12, p. 121102, Dec. 2008.
[5] D. Kasahara *et al.*, "Demonstration of blue and green GaN-based vertical-cavity surface-emitting lasers by current injection at room temperature," *Appl. Phys. Express*, vol. 4, no. 7, pp. 6–9, Jul. 2011.
[6] G. Cosendey, A. Castiglia, G. Rossbach, J.-F. Carlin, and N. Grandjean, "Blue monolithic AlInN-based vertical cavity surface emitting laser diode on free-standing GaN substrate," *Appl. Phys. Lett.*, vol. 101, no. 15, p. 151113, Oct. 2012.
[7] T. Onishi, O. Imafuji, K. Nagamatsu, M. Kawaguchi, K. Yamanaka, and S. Takigawa, "Continuous wave operation of GaN vertical cavity surface emitting lasers at room temperature," *IEEE J. Quantum Electron.*, vol. 48, no. 9, pp. 1107–1112, Sep. 2012.
[8] D. H. Hsieh *et al.*, "Improved carrier injection in GaN-based VCSEL via AlGaN/GaN multiple quantum barrier electron blocking layer," *Opt. Express*, vol. 23, no. 21, pp. 27145–27151, Oct. 2015.
[9] J. T. Leonard *et al.*, "Demonstration of a III-nitride vertical-cavity surface-emitting laser with a III-nitride tunnel junction intracavity contact," *Appl. Phys. Lett.*, vol. 107, no. 9, p. 091105, Aug. 2015.
[10] T. Hamaguchi, N. Fuutagawa, S. Izumi, M. Murayama, and H. Narui, "Milliwatt-class GaN-based blue vertical-cavity surface-emitting lasers fabricated by epitaxial lateral overgrowth," *Phys. Status Solidi A*, vol. 213, no. 5, pp. 1170–1176, May 2016.
[11] K. Ikeyama *et al.*, "Room-temperature continuous-wave operation of GaN-based vertical-cavity surface-emitting lasers with n-type conducting AlInN/GaN distributed Bragg reflectors," *Appl. Phys. Express*, vol. 9, no. 10, p. 102101, Oct. 2016.
[12] G. Weng *et al.*, "Low threshold continuous-wave lasing of yellow-green InGaN-QD vertical-cavity surface-emitting lasers," *Opt. Express*, vol. 24, no. 14, pp. 15546–15553, Jul. 2016.
[13] Y.-S. Liu *et al.*, "Electrically conducting *n*-type AlGaN/GaN distributed Bragg reflectors grown by metalorganic chemical vapor deposition," *J. Cryst. Growth*, vol. 443, pp. 81–84, Jun. 2016.
[14] S. Yoshida *et al.*, "Electron and hole accumulations at GaN/AlInN/GaN interfaces and conductive n-type AlInN/GaN distributed Bragg reflectors," *Jpn. J. Appl. Phys.*, vol. 55, no. 5S, p. 05FD10, May 2016.
[15] M. Arita, M. Nishioka, and Y. Arakawa, "InGaN vertical microcavity LEDs with a Si-doped AlGaN/GaN distributed Bragg reflector," *Phys. Status Solidi A*, vol. 194, no. 2, pp. 403–406, Dec. 2002.
[16] T. Ive, O. Brandt, H. Kostial, T. Hesjedal, M. Ramsteiner, and K. H. Ploog, "Crack-free and conductive Si-doped AlN/GaN distributed Bragg reflectors grown on 6H-SiC(0001)," *Appl. Phys. Lett.*, vol. 85, no. 11, pp. 1970–1972, Sep. 2004.
[17] S. Figge, H. Dartsch, T. Aschenbrenner, C. Kruse, and D. Hommel, "Distributed Bragg reflectors in comparison to RUGATE and nested super lattices – growth, reflectivity, and conductivity," *Phys. Status Solidi C*, vol. 5, no. 6, pp. 1839–1842, May 2008.
[18] E. Hashemi *et al.*, "Effect of compositional interlayers on the vertical electrical conductivity of Si-doped AlN/GaN distributed Bragg reflectors grown on SiC," *Appl. Phys. Express*, vol. 10, no. 5, p. 055501, May 2017.
[19] B.-C. Shieh *et al.*, "InGaN light-emitting diodes with embedded nanoporous GaN distributed Bragg reflectors," *Appl. Phys. Express*, vol. 8, no. 8, p. 082101, Aug. 2015.
[20] C. Zhang, K. Xiong, G. Yuan, and J. Han, "A resonant-cavity blue–violet light-emitting diode with conductive nanoporous distributed Bragg reflector," *Phys. Status Solidi A*, vol. 214, no. 8, p. 1600866, Aug. 2017.
[21] T. Zhu *et al.*, "Wafer-scale fabrication of non-polar mesoporous GaN distributed Bragg reflectors via electrochemical porosification," *Sci. Rep.*, vol. 7, Mar. 2017, Art. no. 45344.
[22] Y. S. Park and J. R. Schneider, "Index of refraction of ZnO," *J. Appl. Phys.*, vol. 39, no. 7, pp. 3049–3052, Jun. 1968.
[23] D. Brunner *et al.*, "Optical constants of epitaxial AlGaN films and their temperature dependence," *J. Appl. Phys.*, vol. 82, no. 10, pp. 5090–5096, Nov. 1997.
[24] H. Karzel *et al.*, "Lattice dynamics and hyperfine interactions in ZnO and ZnSe at high external pressures," *Phys. Rev. B, Condens. Matter*, vol. 53, no. 17, pp. 11425–11438, May 1996.
[25] I. Vurgaftman and J. R. Meyer, "Band parameters for nitrogen-containing semiconductors," *J. Appl. Phys.*, vol. 94, no. 6, pp. 3675–3696, Sep. 2003.
[26] T. Ben-Yaacov, T. Ive, C. G. Van De Walle, U. K. Mishra, J. S. Speck, and S. P. Denbaars, "Properties of In-doped ZnO films grown by metalorganic chemical vapor deposition on GaN(0001) templates," *J. Electron. Mater.*, vol. 39, no. 5, pp. 608–611, May 2010.
[27] H. Y. Xu, Y. C. Liu, Y. X. Liu, C. S. Xu, C. L. Shao, and R. Mu, "Ultraviolet electroluminescence from p-GaN/i-ZnO/n-ZnO heterojunction light-emitting diodes," *Appl. Phys. B, Lasers Opt.*, vol. 80, no. 7, pp. 871–874, Jun. 2005.
[28] D. Adolph, R. R. Zamani, K. A. Dick, and T. Ive, "Hybrid ZnO/GaN distributed Bragg reflectors grown by plasma-assisted molecular beam epitaxy," *APL Mater.*, vol. 4, no. 8, p. 086106, Aug. 2016.
[29] F. Hjort, E. Hashemi, D. Adolph, T. Ive, and Å. Haglund, "Electrically conductive ZnO/GaN distributed Bragg reflectors grown by hybrid plasma-assisted molecular beam epitaxy," *Proc. SPIE*, vol. 10104, p. 1010413, Feb. 2017.
[30] A. Janotti and C. G. Van de Walle, "Fundamentals of zinc oxide as a semiconductor," *Rep. Prog. Phys.*, vol. 72, no. 12, p. 126501, 2009.
[31] A. J. Ptak *et al.*, "Controlled oxygen doping of GaN using plasma assisted molecular-beam epitaxy," *Appl. Phys. Lett.*, vol. 79, no. 17, pp. 2740–2742, Oct. 2001.
[32] F. Bernardini, V. Fiorentini, and D. Vanderbilt, "Spontaneous polarization and piezoelectric constants of III-V nitrides," *Phys. Rev. B, Condens. Matter*, vol. 56, no. 16, pp. R10024–R10027, Oct. 1997.

[33] T. B. Bateman, "Elastic moduli of single-crystal zinc oxide," *J. Appl. Phys.*, vol. 33, no. 11, pp. 3309–3312, Nov. 1962.

[34] T. Hanada, "Basic properties of ZnO, GaN, and related materials," in *Oxide and Nitride Semiconductors: Processing, Properties, and Applications*, T. Yao and S.-K. Hong, Eds. Berlin, Germany: Springer, 2009, pp. 1–19.

[35] C. E. Dreyer, A. Janotti, C. G. Van de Walle, and D. Vanderbilt, "Correct implementation of polarization constants in wurtzite materials and impact on III-nitrides," *Phys. Rev. X*, vol. 6, p. 021038, Jun. 2016.

Filip Hjort received the B.Sc. degree in engineering physics and the M.Sc. degree in applied physics from the Chalmers University of Technology, Gothenburg, Sweden, in 2014 and 2016, respectively, where he is currently pursuing the Ph.D. degree in microtechnology and nanoscience.

His research interests include III-nitride-based vertical-cavity surface-emitting lasers and novel light-emitters emitting in the ultraviolet-blue-green spectrum.

Ehsan Hashemi was born in Tehran, Iran, in 1986. He received the B.S. degree in electrical engineering from the Amirkabir University of Technology formerly called the Tehran Polytechnic, in 2009, and the M.Sc. and Ph.D. degrees in photonics engineering and microtechnology and nanoscience from the Chalmers University of Technology, Gothenburg, Sweden, in 2012 and 2016, respectively.

His research interests include the design and fabrication of GaN-based optical microcavity devices and dielectric-based high contrast metastructures.

David Adolph received the M.Sc. degree in engineering physics from Lund University, Sweden, in 2003, and the Ph.D. degree from the Chalmers University of Technology, Gothenburg, Sweden, in 2016. His thesis work involved the growth of ZnO/GaN distributed Bragg reflectors by plasma-assisted molecular beam epitaxy.

His current research interests involve epitaxial growth and characterization of III-Nitride layers for photonics and microwave electronics.

Tommy Ive received the Ph.D. degree in physics from the Humboldt University of Berlin, Germany, in 2005. In 2010, he started as an Assistant Professor and later as an Associate Professor with the Chalmers University of Technology, Gothenburg, Sweden.

Olof Bäcke received the Ph.D. degree in physics from the Chalmers University of Technology, Gothenburg, Sweden, in 2015. He is currently a Post-Doctoral Researcher with the Chalmers University of Technology.

His research interests are focused on using electron microscopy to explore the connection between the microstructure of a material and its properties.

Mats Halvarsson received the Ph.D. degree in physics from the Chalmers University of Technology, Gothenburg, Sweden, in 1994. He is currently a Professor with the Department of Physics, Chalmers University of Technology.

His research interests include advanced electron microscopy and micro-analysis of materials, linking fabrication and service to the materials microstructure and properties. Materials of interests include metals, ceramics, alloys, and composites.

Åsa Haglund received the M.Sc. degree in physics from Gothenburg University, Sweden, in 2000, and the Ph.D. degree in electrical engineering from the Chalmers University of Technology, Gothenburg, Sweden, in 2005.

She is currently an Associate Professor with the Chalmers University of Technology, where she is focusing on III-nitride-based optoelectronic devices, in particular resonant light-emitters in the ultraviolet-visible regime. She has published over 100 papers. Her scientific background is in the area of GaAs-based lasers emitting in the infrared regime, including high modulation speed and nanostructures for transverse mode and polarization control. She is an Associate Editor of the *IET Electronic Letters*.

Dr. Haglund has co-organized the European Semiconductor Laser Workshop 2017, the international conference Graphene Week, and the Optics and Photonics in Sweden.